Attenuation of slow (10–40 eV) electrons in soft nanoparticles: Size matters in argon clusters

Mathias Winkler* and Knut J. Børve†
Department of Chemistry, University of Bergen, NO-5007 Bergen, Norway

(Received 10 March 2017; published 10 January 2018)

Electron attenuation due to inelastic and elastic scattering in condensed media can often be described in terms of the effective attenuation length (EAL) of the electron. The EAL is thus an important parameter for describing electron transport processes as exemplified by dissipation of energy following radiolysis. Focusing on electrons at low electron kinetic energies (10–40 eV) in condensed argon, we determine EAL from x-ray photoelectron spectra of argon nanoparticles and compare to values obtained from valence ionization in thin argon films as well as from gas-phase electron-scattering data. EAL determined from argon clusters shows variation with cluster size. Moreover, the values are significantly lower than those obtained in valence-ionization studies and from scattering data. Our results corroborate recent x-ray photoelectron spectroscopy–based determination of EALs of water showing large differences to the EALs determined by other methods in amorphous ice at low kinetic energies of the photoelectron [Y.-I. Suzuki, K. Nishizawa, N. Kurahashi, and T. Suzuki, Phys. Rev. E **90**, 010302 (2014)], underlining that care must be taken when using EAL values from other sources for core-level electrons.

DOI: 10.1103/PhysRevE.97.012604

I. INTRODUCTION

Transport of energetic electrons through bulk matter is of great importance in several branches of technology as well as radiation biology. One important aspect of electron transport is the inelastic mean free path (IMFP), which is the mean distance traveled by an electron before undergoing inelastic scattering. A closely related concept that takes into account the extension of electron trajectories through elastic scattering is the effective attenuation length (EAL). EAL enters all kinds of electron spectroscopy including that of x-ray photoelectron spectroscopy (XPS). More specifically, XPS, which is the most widely used technique for chemical analysis of the outermost few nanometers of solid surfaces [1], owes its surface sensitivity to the relatively short effective attenuation length of the emitted photoelectron. Moreover, since EAL depends on the kinetic energy of the electron, *e*KE, the probing depth may be controlled by changing the x-ray wave length. Recent technical developments have turned this principle into a powerful tool for depth profiling of matter [2].

For electrons with *e*KE in the range 50–2000 eV, the IMFP and the EAL are quite well established. In this energy range, IMFPs and EALs are available from databases [3,4] for many materials. For *e*KE below 50 eV fewer data are available because both measurements and the theoretical description of electronic scattering become more challenging. However, this low-*e*KE region is of interest in many areas. For instance, in living matter, the energy of ionizing radiation is largely deposited as secondary electrons with kinetic energies in the 1- to 20-eV range, which is suggested to play a crucial role in the radiolysis of DNA [5]. Regarding the surface sensitive electron spectroscopies, the shortest EALs and thus highest surface senitivities are often found at low *e*KEs [6,7].

In order to obtain quantitative rather than only qualitative information about the depth profile, the effective attenuation length of the photoelectron has to be known accurately. Recently, XPS has been used to determine the EAL of liquid water by different research groups [8–10]. However, there is noticeable disagreement between these studies, as well as with EAL-IMFP data from amorphous ice obtained from electron backscattering [11] and from overlayer technique [12] experiments. For instance, at a kinetic energy of 30 eV the estimates for the EAL range approximately from 5 to 50 Å [10].

New approaches use photoemission studies of nanoparticles [13,14] and aerosols [15,16] to measure electron attenuation at low *e*KE in soft matter. Clusters made up from rare-gas atoms or closed-shell molecules are simple in the sense that the electronic structure changes only weakly and gradually with cluster size. Because of these properties, clusters from argon may serve as a reference system and are investigated in this study with respect to their effective attenuation lengths of photoelectrons. Here we focus on the kinetic energy region from 10 to 40 eV, where one generally expects to find the largest variation of the EAL with the kinetic energy, with a minimum for the EAL around 20–40 eV and a steep increase at kinetic energies below that minimum. One may note that in the case of water the largest discrepancies of EAL estimates among different studies and methods fall into this region close to threshold [10].

An earlier XPS study of rare-gas clusters using the same experimental setup was undertaken by Tchaplyguine *et al.* [17]. They report bulk-to-surface signal ratios for argon, krypton, and xenon clusters in the kinetic energy region from 10 to 160 eV. From these signal ratios EALs can be estimated in connection with cluster size estimates from general scaling laws. Amar *et al.* [18] used theoretical line shapes based on cluster models rather than the simple bulk-to-surface ratio for estimating the EAL but likewise relied on the size estimate of the scaling law. In the present study, both the size and the

*Current address: Department of Physics, Norwegian University of Science and Technology, NTNU, N-7491 Trondheim, Norway; mathias.winkler@ntnu.no
†knut.borve@uib.no

TABLE I. Experimental settings (stagnation pressure p_0, nozzle temperature T_n) and estimated cluster size N_{est}. Uncertainty in the last digit is given within parentheses.

Expt.	p_0 (bar)	T_n (K)	N_{est}
A	1.94(1)	303(1)	≈900
B	2.94(1)	289(1)	≈1800
C	1.51(1)	127(1)	≈14 000

EAL are estimated from theoretical line shapes, thus building a more consistent basis for comparison of the EAL for different cluster sizes.

II. EXPERIMENTAL DETAILS

Argon clusters were produced in a supersonic beam expansion using a setup [17] at beamline I411 at the MAX-lab synchrotron facility in Lund, Sweden. Gaseous argon is expanded through a nozzle with an opening diameter of 150 μm and a half-opening angle of 10° into a low-pressure chamber. This results in a strong temperature drop and cluster formation. The beam characteristics are enhanced by means of a skimmer (diameter 300 μm) between the expansion chamber and the analyzer chamber where the beam is probed by photoelectron spectroscopy.

Clusters were produced under three different expansion conditions (A–C) using stagnation pressure and nozzle temperature as summarized in Table I. At each expansion condition, Ar2p photoelectron spectra were recorded at several photon energies between 260 and 290 eV. The total instrumental resolution was 110–130 meV, varying slightly with photon energy. The hemispherical electron analyzer (Scienta R4000) was set to 54.7° with respect to the polarization plane of the photon beam. Energy calibration is achieved by setting the $2p_{3/2}$ ionization energy of gaseous argon to 248.629(20) eV [19].

III. THEORETICAL MODELS

A. Lineshapes from realistic cluster models

In this study we take advantage of a recently described approach [14] to the simultaneous determination of size and attenuation length of clusters, based on line-shape modeling of core-level photoelectron spectra. The line-shape models are based on data from molecular dynamics (MD) simulations conducted with the TINKER molecular modeling package version 5.1 using van-der-Waals and atomic-polarizability parameters for argon as provided with the AMOEBA force field [20,21]. Clusters of various sizes are simulated at a finite temperature (40 K) using the canonical (NVT) ensemble with a time step of 5 fs, an equilibration phase of at least 0.5 ns, and a total simulation time of 1 ns or longer.

The simulation temperature (40 K) is close to the estimate of 37 K for argon clusters with sizes $N > 800$ [22]. The present force field reproduces the density of solid argon at 40 K exceptionally well [23].

Rare-gas clusters undergo several structural transitions as a function of cluster size, and while approximate size regimes are known, the exact transition sizes are still under debate [24]. We have used two different choices of initial cluster structures in our MD simulations: icosahedral and octahedral (fcc) structures. Icosahedral starting structures were used in simulations for sizes 55, 147, 309, 561, 923, 1415, 2057, and 2869. Correspondingly, simulations with cuboctahedral initial cluster structures were conducted for sizes 55, 147, 309, 561, 923, 1415, 2057, 2869, 6525, 8217, 10 179, 12 431, 14 993, and 17 885. While these cluster sizes correspond to closed-shell structures, deviations from ideal structure occur during the MD simulations. We realize that several other structural modifications (in particular, decahedral) may be of relevance at intermediate cluster sizes [25]. On the other hand, diffraction patterns of clusters can only be explained by the presence of both fcc and hcp stacking of atoms [26].

During the production phase of the MD simulation, for each combination of cluster size and choice of initial cluster structure, snapshots of the cluster structure are taken at intervals of 1 ps. In each of these cluster geometries, a binned distribution of cluster-to-monomer shifts (ΔIEs) is prepared in a loop over all atoms in the cluster; computing the shift in $2p$ ionization energy (relative to that of the free atom) as well as an intensity based on the position in the cluster and a predefined EAL value [18]. The spacings between different EAL values used for the calculation of ΔIE distributions were 0.25, 0.5, and 1 Å for EAL values below 11 Å, between 11 and 15 Å, and above 15 Å, respectively. The site-specific ΔIE is formed by replacing the atom in question with the corresponding positively charged ion and computing the resulting polarization energy in the cluster. The AMOEBA force field employs a mutual polarization scheme that allows for accurate and self-consistent calculation of induced atomic dipole moments. At the end of each run, a time-averaged distribution of ΔIEs is formed and convoluted by an atomic shape function that accounts for lifetime broadening (118(4) meV [27]) and postcollision interactions (PCI) [28]. Since the PCI effect depends on the relative kinetic energy of the photoelectron and the Auger electron, the atomic line shape employs different PCI parameters for surface and bulk atoms. In addition to the difference in kinetic energy between photoelectrons emitted from the bulk and from the surface, Lindblad *et al.* [29] found that PCI for bulk photoelectrons is dampened by the dielectric response of the material. They proposed to scale the PCI parameter [28] by the relative permittivity of the medium, which in the case of argon is 1.61 [29]. This correction is adopted here.

B. The fitting procedure

The cluster parts of the experimental spectra are analyzed in terms of theoretical line shape models that correspond to specific choices of cluster size and electron attenuation length. As there is some overlap between cluster and monomer signals, the experimental spectra were first fitted using a purely empirical model in order to account for the monomer signal independently from the cluster models. In this preprocessing procedure, the Ar2p spectrum is considered to consist of six components, namely the $j = 1/2$ and $j = 3/2$ spin-orbit doublet for atoms in the gas phase, atoms at the surface of clusters and atoms in the bulk of clusters, respectively. Each component is represented by the convolution of a Gaussian function and the PCI function defined in Ref. [28]. In each case, the PCI parameter is calculated according to the kinetic

energy of the photoelectron. Additionally, for the bulk doublet, the PCI parameters are scaled according to Ref. [29]. When fitted to the experimental spectra, the atomic spin-orbit splitting (2.13 eV [30]) was used as constraint for each doublet and, moreover, the lifetime width and PCI parameters were held constant. This leaves the following 15 parameters to be determined in the fit to experiment: the Gaussian width of the monomer doublet (which represents the instrumental broadening of the experiment), six peak intensities, three energy positions (one for each doublet), four Gaussian widths for the two cluster doublets, and a linear background. Following this procedure, the position, intensities, and width of the monomer peaks are determined for each of the three experiments.

In the subsequent analyses of cluster spectra, the monomer signals are represented as described above, with fixed parameters. The cluster signal, however, is treated differently in that no assumption of surface and bulk components were made, but rather a distribution of $2p$ ionization energies (relative to that of the atom) was employed as obtained from MD simulations (see above for details), corresponding to a specific cluster size and a specific EAL. The cluster model was convoluted by a Gaussian distribution to allow for experimental broadening, possible effects from the cluster-size distribution in the experiment (i.e., apart from the mean size), and interatomic Franck-Condon effects beyond those included in the distribution of initial-state structures. The intensity and Gaussian width of these modeled cluster line shapes were optimized with separate values for the two spin-orbit components. A least-squares fitting routine [31] was used for all tasks described in this section.

C. FEFF calculations

In order to study the effect of electron backscattering on the photoionization cross section, x-ray absorption near-edge structure (XANES) calculations were conducted by means of the program FEFF (Version 9.6) [32]. In these calculations, icosahedral and octahedral (fcc) clusters containing 55 and 147 atoms were studied in their optimized structures as obtained from the AMOEBA force field.

IV. RESULTS AND DISCUSSION

In this section we will first present estimates for the cluster sizes and EAL based on line shape modeling for expansion experiments A–C. As we shall see soon, the EALs differ significantly between these experiments, i.e., EAL depends on cluster size. We then compare our values to existing data for argon in the gas and condensed phases, before discussing possible explanations for our observations.

A. Size and EAL estimates from XPS spectra

A typical Ar$2p$ photoelectron spectrum recorded during these experiments is shown in Fig. 1. The monomer signal at around 248.6 eV and the cluster signal around 247.9 eV are associated with the $2p_{3/2}$ spin-orbit component and are shifted by 2.13 eV to lower binding energies compared to the corresponding $j = 1/2$ components. The cluster signal exhibits well-defined structural features that can be assigned to atoms at the surface and atoms in the bulk of the clusters. The solid line in the figure represents our theoretical model

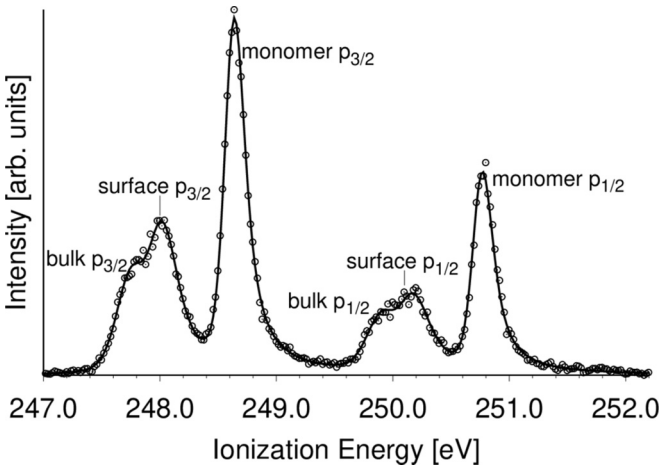

FIG. 1. Argon $2p$ photoelectron spectrum of argon clusters produced in experiment B (see Table I) at a photon energy of 279 eV. The open circles are experimental data points while the solid line represents a line-shape model based on a time-averaged distribution of ionization energies (cluster-to-monomer shifts) computed for an $N = 2057$ ($2p_{3/2}$) and $N = 923$ ($2p_{1/2}$) icosahedral cluster. The model uses EAL values of 7.5 and 9 Å for $2p_{3/2}$ and $2p_{1/2}$, respectively.

fitted to the experimental data (open circles), as described under Section III. The fit is excellent given that the line-shape model is based on appropriate values for the cluster size and effective electron attenuation lengths (different ones for $2p_{3/2}$ and $2p_{1/2}$). Notably, the size estimates based on the different spin components are $N = 2057$ and $N = 923$, illustrating the uncertainty. Nevertheless, the EAL values differ by only 1.5 Å.

In Fig. 2, we show spectra for the three different experiments, recorded at nearly identical photon energies. In experiments A–C, one can observe that with increasing mean cluster size, the magnitude of the cluster-to-monomer shift increases, as does the bulk fraction. Figure 3 illustrates this point for model spectra. It is thus evident that XPS spectra contain information about cluster size as well as about the EAL

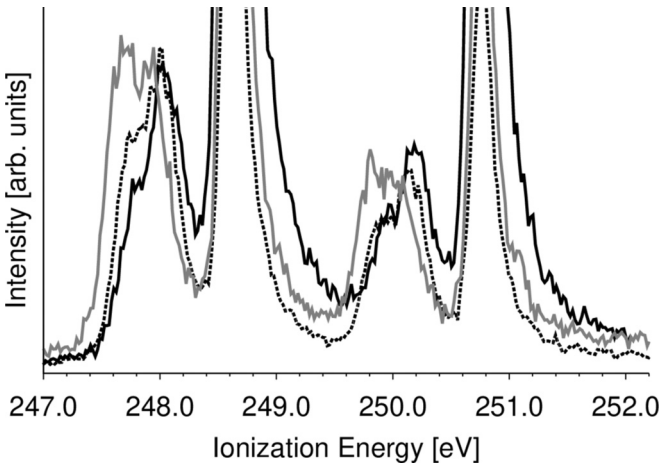

FIG. 2. Ar2p photoelectron spectra of argon clusters produced under three different experimental conditions A (solid black), B (dotted black), and C (gray). The spectra are recorded at a photon energy of about 280 eV (kinetic energy ≈ 30 eV).

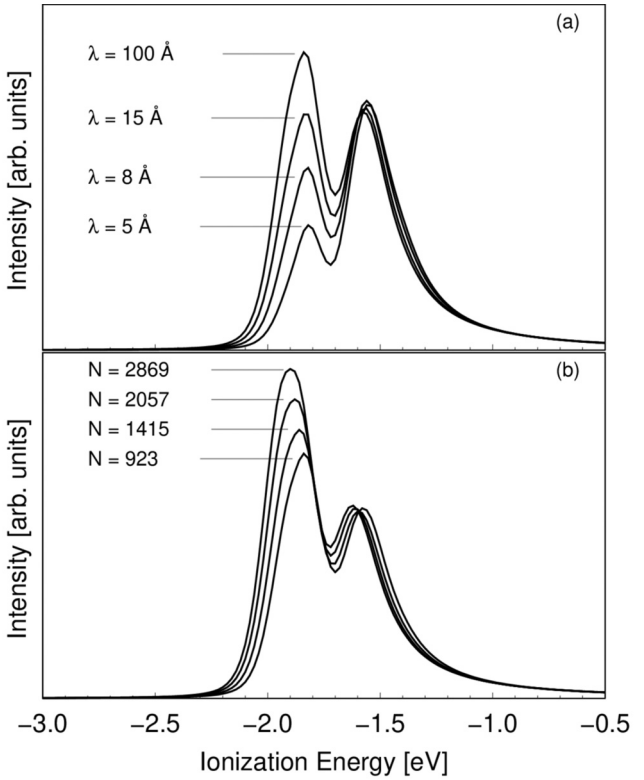

FIG. 3. Model spectra illustrating (a) EAL dependence and (b) size dependence of the cluster spectra.

of the photoelectron. To extract this information, we proceed as outlined in the following and further detailed in Ref. [14].

Theoretical model Ar2p spectra are prepared for a range of cluster sizes (N) and EAL, with additional parameters left to be determined in a fit to experiments, Sec. III for a complete account. The fitting parameters describe intensity, width, background, and overall energy calibration but do not affect relative energies nor the peak structure. Each of these models are fitted to the spectra from each of experiments A–C. Associated with each experimental spectrum, one obtains an optimal fit and the corresponding goodness-of-fit measure for each combination of assumed mean cluster size and EAL value, i.e., $\chi^2 = \chi^2(N,\mathrm{EAL})$. Using experiment C as an example, Fig. 4 shows the resulting goodness-of-fit parameter χ^2 as a function of EAL for different values of N. Clearly, model spectra based on some mean cluster sizes give significantly better fits to that spectrum than do others. For most choices of N, the χ^2 function increases rather sharply outside a narrow range of EAL values. Furthermore, Fig. 4 shows the envelope of the χ^2 function as generated by the models that give the best fit for each choice of EAL. By identifying the minimum of this envelope, the best estimates of both the EAL and cluster size are obtained for the experiment underpinning the fit.

As it turned out, spectra of A and B are significantly better fitted with line shapes obtained from icosahedral cluster models. Therefore, in these cases EAL and size estimates pertaining to the icosahedral model are reported, while the estimates for **C** are based on the cuboctahedral (fcc) model.

The size estimates of each experimental series are shown in Fig. 5 as a function of kinetic energy of the photoelectron.

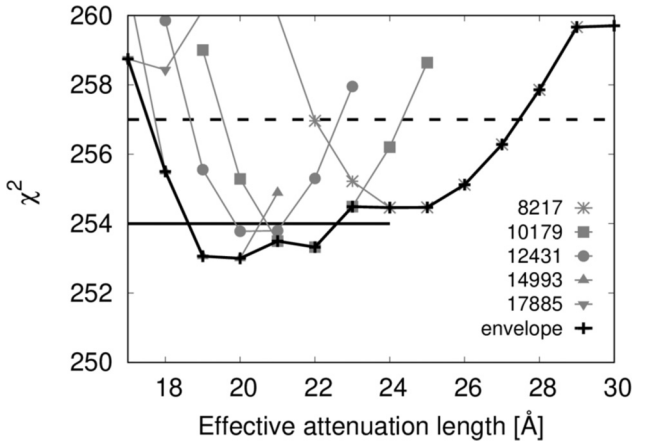

FIG. 4. χ^2 obtained in the fitting of different theoretical model spectra to experimental Ar2p spectrum C at 11.8 eV kinetic energy of the photoelectron. The model spectra were generated for different simulated cluster sizes (listed in the figure) and for a variably spaced grid of effective attenuation lengths as indicated by markers. The horizontal lines indicate the 1-σ (solid) and 2-σ (dashed) confidence levels.

The size estimates do not vary systematically with the kinetic energy, demonstrating that our size estimates are independent of the EAL values (which do vary systematically with the kinetic energy). The overall size estimates obtained as the mean of estimates for each spectrum taken (see Fig. 5) are $N \approx 900$, $N \approx 1800$, and $N \approx 14\,000$ for experiments A, B, and C, respectively. These estimates are significantly larger than mean sizes estimated from empirical scaling laws [33–35] which are $\langle N \rangle \approx 100$, 270, and 2700 for experiments A–C, respectively. While these scaling laws are frequently used, it has been realized early that size estimates may differ by a factor of two using the same method of size determination and that they may differ by a factor of three between methods [34]. More recent studies find that scaling law estimates may differ by a factor of five for different geometries of conical nozzles [36] and deviation of two orders of magnitude towards smaller sizes have been reported by others [37]. Our findings are more in line with studies based on photoelectron spectroscopy,

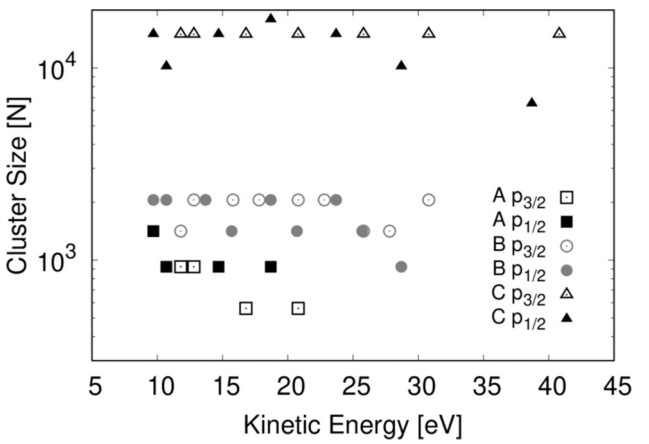

FIG. 5. Size estimates for the spectra of A–C. The data points show the cluster size of the MD model that yielded the best fit in each case.

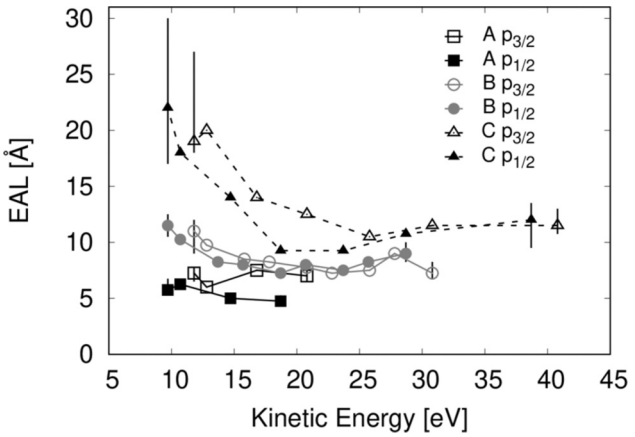

FIG. 6. EAL estimates obtained by line-shape modeling for three different experiments yielding cluster of sizes $N \approx 900$ (A, triangles), $N \approx 1800$ (B, circles), $N \approx 14\,000$ (C, squares). Two data series are shown for each experiment: one from fits to the Ar2$p_{3/2}$ signal (open symbols) and the other from fits to the Ar2$p_{1/2}$ (full symbols). The 2-σ standard error is indicated with bars for the lowest and highest electron kinetic energy of each series.

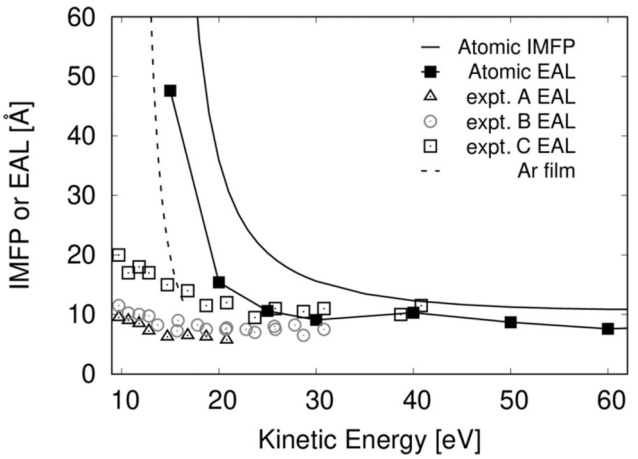

FIG. 7. Comparison between EALs as estimated in experiments A–C and inelastic-mean-free paths (IMFP) and EAL estimates from electron scattering data of atomic argon (gas-phase) and argon film. IMFP are obtained by using the empirical formulas for the electron impact excitation and ionization cross sections given in Eqs. (3) and (5) in Ref. [45]. These are added to give the total inelastic electron-scattering cross sections which are combined with a density of 1.74 g/cm^3 to calculate the IMFPs. Using the same density, the transport mean-free path has been calculated from momentum transfer cross-section data from Ref. [46]. The atomic EALs were calculated with these data using the empirical formula given in Ref. [47]. The mean-free path in argon films is from Eq. (8) in Ref. [48], only mapped to the kinetic energy scale by subtracting the ionization threshold cited in that study.

electron diffraction, and buffer-gas collision, which report cluster sizes that are larger than those estimated by the scaling laws [38–44]. Since those differences in cluster size estimate may to a considerable part stem from the source condition, it is useful to compare our size estimates with previous results from studies using the same cluster source. Reference [17], using the very same cluster source and detection technique (Ar2p XPS) as in the present study, found that for argon clusters produced at stagnation conditions that would indicate a mean cluster size of $\langle N \rangle = 300$ from scaling laws, the observed surface-to-bulk ratio was around 1 at a kinetic energy of 150 eV. At this high kinetic energy, the inelastic mean-free-path (IMFP) from atomic data can be taken as a tight upper bound to the EAL at about 11 Å. With this value for EAL, one needs to consider cluster models in the range of 1400–2100 atoms in order to obtain a surface-to-bulk ratio of unity. This size estimate is close to what we present for experiment B, for which scaling laws give $\langle N \rangle \approx 270$ cluster. Thus our size estimates are consistent with earlier observations with this particular cluster source.

In Fig. 6, we show EAL estimates as a function of photoelectron kinetic energy for the three experiments. The estimated EAL is found to vary with cluster size such that at all kinetic energies explored, the smallest cluster has the shortest EAL and the largest cluster has the longest EAL. Given the number of data points, this observation is clearly not due to happenstance. Moreover, while icosahedral cluster models were used in fits to A and B as opposed to cuboctahedral models in C, tests show that cuboctahedral models would have given even lower (if only by 1 Å) EAL estimates for A and B than did the icosahedral models, showing the persistency of the described pattern. See Appendix A for a more detailed review of possible systematic errors.

B. Comparison to EALs and IMFPs from atomic cross-ection data and solid argon

Clusters form the link between the gas and condensed phases, and as a stepping stone to our discussion of possible causes for the observed cluster-size dependency in the electron attenuation length, we shall compare our EAL values to data for atomic argon as well as for argon films.

Comprehensive data sets are available for argon-electron scattering [49,50] that may be used for estimating mean free paths for inelastic scattering and EAL for the given mass density of the cluster. There are empirical formulas that summarize these data, and Powells' EAL model [47] is plotted in Fig. 7 together with our estimates. There are rather large discrepancies between the atom-based EAL and our values in the region of 10- to 20-eV electron kinetic energy (eKE). On the other hand, these estimates are comparable above an eKE of 25 eV, i.e., where the IMFP and EAL curves have already flattened out. Agreement in this energy region is corroborated by our previous studies that found good agreement between EAL values obtained from photoemission data for molecular clusters, on the one hand, and EAL estimates formed on the bases of molecular electron-scattering cross sections, on the other, at kinetic energies of 30 eV (CS_2, Ref. [13]) and 40 eV (C_2H_6, Ref. [14]).

Returning to the disagreement between the atom- and cluster-based EAL at kinetic energies below 20 eV, several reasons are conceivable. First, since valence ionization makes the largest contribution to inelastic scattering in this energy range, the lowering of the valence ionization potential that is known to take place in clusters will act to increase the probability of inelastic scattering. Second, the first optical excitation is likely to occur at lower energies in the cluster

compared to the atom, again increasing the inelastic scattering cross section compared to that of the free atom.

Turning to condensed argon, data on inelastic electron scattering are scarce and we are only aware of two studies that report IMFPs or inelastic scattering probabilities at low *e*KE in argon films formed on a metal substrate [48,51]. The study of Keszei *et al.* [51] using low energy electron transmission found inelastic scattering probabilities to be negligible in the *e*KE range between 1- and 4 eV, save for a peculiar feature that they assign to impurities or possible film-substrate effects. The electron mean free paths from vacuum ultraviolet photoemission experiments by Schwentner [48] are measured for kinetic energies between 12 and 16 eV and are included in Fig. 7 as a dotted line. Clearly, they show a similar steep rise at low *e*KE as do the atomic data, only shifted to even lower energy, consistent with the red-shifted ionization potential in solid argon.

In contrast to atomic and condensed-film data, the EAL curves from our measurements increase only weakly as the kinetic energy is reduced from 20 to 10 eV. The explanation for the difference in dependency on *e*KE should be sought in processes that are specific to XPS, as opposed to transmission of electrons in the absence of deep-lying holes. More specifically, Lundwall and coworkers [52] reported evidence for photoelectron recapture following Auger decay of core holes in argon clusters. Recapture persisted at least up to 280 eV photon excitation energy, corresponding to *e*KE $\approx$ 32 eV. Noteworthy, while recapture can also be observed for the free argon atom [53], it is negligible for excitation energies above 252 eV photon energy (*e*KE $\approx$ 4 eV) [54,55]. Of course, recapture is not an issue for the argon film data discussed above, since it is obtained from valence photoemission. In addition to these electronic processes one has also to consider the possibility of differences in photoionization cross sections between bulk and surface atoms in the cluster. Similar considerations applies to differences between EALs estimates for the different cluster sizes, to which we turn next.

C. Photoionization cross section vs. electron scattering cross section

We will now discuss possible factors that may account for the size dependence in the EAL estimates. This size dependence does not necessarily suggest that photoionization or electron-scattering cross sections are different for atoms in clusters of different size. While multiple-scattering effects are known for very small argon clusters [56,57], it is perhaps unlikely that differences persist to the larger clusters that have been probed in this study. It seems more plausible that cross sections for surface and bulk atoms differ and that the impact of this difference varies with surface fraction and thus cluster size.

Photoionization cross sections may be affected by electron backscattering, an effect utilized in XANES spectroscopy. Briefly explained, the outgoing photoelectron wave may be backscattered by surrounding atoms and interfere with itself, leading to constructive or destructive interference, and is thus changing photoionization probabilities. The importance of this effect for XPS of molecules in the gas phase has recently been realized [58]. In order to estimate the importance of electron backscattering for the present study we performed multiple-scattering calculations for argon clusters containing 55 and 147 atoms. In each of these clusters we chose to probe three different sites: the center atom, a vertex site at the surface, and a site just beneath the surface (the calculated photoabsorption spectra are provided in Appendix B). We found that there is a considerable impact of the surrounding from threshold to about 10 eV kinetic energy. However, at kinetic energies above 10 eV, i.e., the region which is relevant for our present discussion, almost no differences between the surface sites and the bulk sites are predicted by the calculations.

A further effect to consider is diffraction of the photoelectron. However, taking into account that our clusters are randomly oriented in space and that the asymmetry factor for Ar2p photoionization is rather small ($\beta = 0.2$–0.5) in the relevant energy range [59], this should be highly unlikely. Furthermore, alteration in signal intensity between bulk and surface sites due to elastic scattering smearing out the angular dependency of photoelectrons from the bulk is avoided by recording spectra with the electron analyzer set at the magic angle relative to the polarization plane of the x-ray beam.

Having established that there are no significant differences in photoionization cross sections, we now consider electronic scattering processes, for which it is useful to distinguish losses due to intrinsic (shake-up) and extrinsic (electron transport) processes [60]. The intrinsic process refers to simultaneous excitation of a valence electron on core ionization, while extrinsic losses take place later when the photoelectron is traveling through the medium. Important to note, the main peaks in XPS derive from "non-shaken-up" states, i.e., the signal comes from atoms that are core ionized but otherwise left in their electronic ground state (that is, of course, prior to any decay of the core hole). This means that the observed XPS surface-to-bulk ratio will be affected if cross sections for shake-up are different for surface and bulk atoms.

Intensity loss in XPS due to the core hole and the presence of a surface has been discussed rather extensively in the context of metals and semiconductors [60,61]. These models take into account interactions between the photoelectron and the static core hole, as well as interaction with matter while the electron is traveling in vacuum in the proximity of the surface. A more recent study [62] extended the study of signal loss due to these effects to oxides. It was found that the loss in insulators is somewhat larger than in metals, mainly due to an increase in intrinsic bulk losses. Losses that arise from the electron-surface interactions, on the other hand, were found to be negligible due to the larger band gap. The size of these two contributions also depends on the kinetic energy of the electron, as slower electrons have more time to interact with the surface [60]. Likewise, there is a dependence on the emission angle, as the electron stays longer in the vicinity of the surface at smaller emission angles. When carrying the conclusions from these studies over to the present system of argon clusters, we note that the kinetic energies of our electrons are much smaller (10–40 eV) than those considered in the studies referred to above (300–1000 eV) and this warrants some caution. Nevertheless, it seems reasonable to infer that surface excitation is probably negligible because of the large band gap in argon, combined with a relatively low polarizability. On the other hand, it is suggested that the intrinsic losses ("shake-up") play a major role in oxides and insulator-like systems.

While intrinsic effects may play a role in our observations, it cannot explain the entirety of the data. This is because valence excitations are not energetically available at the lowest kinetic energies that we consider. The band gap of argon films is estimated to be 14.3 eV [63], well above our lowest photoelectron kinetic energy of 9.7 eV. This kinetic energy is even lower than the lowest band gap reported for argon in the literature, which is 11.4 eV, calculated for hexagonal argon [64]. In the same study the band gap for cubic argon to 14.0 eV was computed, in good agreement with experiment. Ar2p shake-up satellites are observed from 17 eV above the Ar2$p_{3/2}$ threshold for atomic argon [59].

Finally, we shall return to the discussion of photoelectron recapture in clusters as reported by Lundwall *et al.* [52]. From the Auger spectra presented in their study, at a low excitation energy of 258 eV (corresponding to 10 eV kinetic energy for the photoelectron) the signal corresponding to recapture is stronger than that from normal Auger. At a higher excitation energy of 280 eV (eKE = 32 eV) the recapture signal has still 25% of the intensity of the normal Auger signal as estimated from peak heights. Given the importance of the effect and the indication by Lundwall *et al.* [52] that the process is more likely to occur in the bulk than at the surface, this is the best explanation for the observed differences in EAL between experiments A–C.

V. CONCLUSIONS

We have estimated the EAL for photoelectrons in argon clusters based on line-shape modeling of 2p photoelectron spectra. In the studied range of 10–40 eV kinetic energy of the photoelectron, we found systematic differences between our estimated EAL values for the different cluster sizes, with EAL increasing with increasing cluster sizes. The differences in EALs are more pronounced for lower kinetic energies.

Compared to data for Ar films (studied by VUV photoemission), the EALs in this study are much smaller below about 16 eV kinetic energy. Comparing to EALs estimated from electron-scattering cross sections of the free argon atom, we find that the EALs are comparable at kinetic energies above 25 eV (but not below), suggesting that the so-called gas-phase approximation is reasonable from this point upwards to higher kinetic energies.

We explore possible factors that may account for the size effect and the observed differences compared to the Ar film data. While electron backscattering gives rise to differences in the photoionization cross section for bulk and surface sites below 10 eV in kinetic energy, this effect is found not to be important for argon in the energy range used in the experiments (10–40 eV). Neighbor-induced photoelectron recapture is identified as the most likely process to explain the cluster-size dependency that is observed in EAL. Conversely, the present finding of cluster-size dependency in the electron attenuation length confirms the importance of neighbor-induced recapture of photoelectrons following Auger decay of a core hole.

ACKNOWLEDGMENTS

We express our great gratitude to Leif Sæthre, Andreas Lindblad, Velaug Myrseth Oftedal, and Jarle Harnes for help in conducting the experiment. We are pleased to thank Maxim Tchaplyguine for his assistance during beamtime and the Nordic Research Board (NORDFORSK), the Norwegian High Performance Computing Consortium NOTUR (Grant No. NN2506K), and the EC Transnational Access to Research Infrastructure Program (TARI) for support.

TABLE II. Results from fits of line-shape models of different cluster sizes allowing the cluster-to-monomer shift to vary. Ar2$p_{3/2}$ spectra from experiment A at photoelectron kinetic energies of eKE = 20.8 and eKE = 11.8 eV were fitted. (See text for more details.)

N	923	561	309	147
		eKE = 20.8 eV		
ΔE (meV)	1	−18	−36	−103
EAL (Å)	5	5.5	7.5	9
		eKE = 11.8 eV		
ΔE (meV)	11	−11	-32	−104
EAL (Å)	7.75	9	14.5	—

APPENDIX A: ERROR SOURCES AND THEIR IMPACT ON THE ESTIMATED EFFECTIVE ATTENUATION LENGTH

The primary source of overestimation of the cluster size would be through underestimation of the magnitude of the cluster-to-monomer shift (ΔIE). The atomic polarizability of argon used in the force field model is within 0.1% of the experimental one, which is measured to an accuracy of 0.05% [65]. The polarization response also depends on the number density of the material. We conducted an MD simulation of fcc argon using periodic boundary conditions at 40 K and found that the experimental density [23] is reproduced to within 0.02%. Combined with the present use of an accurate mutual polarization model, this would suggest that the error in mean cluster-to-monomer shift is in the order of 1 meV.

Clusters of different sizes may have somewhat different temperatures, and we have seen previously [14] that this affects the observed photoelectron spectrum through the number density and thus the polarization energy in the ionized state. However, the thermal expansion coefficient of argon is very small with density changes of less than 1% over a temperature span of 10 K [23]. Thus, since the temperature difference between the clusters produced in experiments A–C can be expected to be smaller than 10 K [22,43], which in turn is expected to introduce a relative error of 1.3% in ΔIE (the polarization energy scales with the power of 4/3 of the material density), corresponding to less than 10 meV.

In order to explore whether errors of this size may affect our result qualitatively, some fits were repeated using smaller cluster sizes and releasing the constraint on the energy position of the clusters, i.e., allowing the cluster-to-monomer shift to vary freely in the fitting. The displacement in energy determined in the fit then indicates how large the systematic error has to be before the cluster size used in the fit would be favored. Results for two examples pertaining to experiment A, i.e., the experiment in which the smallest clusters were produced, are shown in Table II. For example, when employing a line shape as computed for a $N = 309$ cluster in the fit, the cluster model is shifted slightly more than 30 meV toward lower ionization energy. Put differently, for $N = 309$ to be

identified as the correct mean cluster size, our theoretical cluster-to-monomer shifts would have to increase by 30 meV in magnitude, i.e., become significantly more negative. And still, even with this smaller size, the estimated EAL would be 7.5 and 14.5 Å for photoelectrons with kinetic energies of 20.8 and 11.8 eV, respectively. These values are considerable smaller than the corresponding values for experiment C, which are 12.5 and 19 Å. Finally, it should be noted that systematic errors in the calculation of the cluster-to-monomer shift would affect all size estimates in the experimental series A–C in the same direction and hence also the EAL estimates. Thus it is established that an overestimation of the cluster size cannot be responsible for the observed size dependency of EAL, although it may contribute.

Another possible source of systematic errors may be the asymmetry parameter accounting for the PCI of the photoelectron with the Auger electron, which is emitted in the main decay process of the core-hole. This parameter depends on the kinetic energy and is thus somewhat different for photoelectrons emitted from the surface and the bulk of the cluster. However, Lindblad *et al.* [29] discovered that the bulk signal shows much less asymmetry than the surface and suggested that the bulk PCI factor is scaled with the inverse relative permittivity of the material. It is argued that this is because the photoelectron is overtaken by the Auger electron within the cluster and the additional charge is screened by the cluster medium. Thus it has been speculated that the correction factor may be size dependent with smaller clusters showing a more asymmetric bulk signal. The cluster size as estimated by a scaling law in that study is $\langle N\rangle \approx 1600$, which is in between the scaling-law sizes in experiments B ($\langle N\rangle \approx 270$) and C ($\langle N\rangle \approx= 2700$). As the PCI effect becomes more important with decreasing kinetic energy of the photoelectron, tests were undertaken for spectra recorded at $h\nu = 261$ eV by refitting the spectra without the proposed correction. In all of these cases, the fits without the permittivity correction became significantly worse. For instance, for the medium-size clusters in experiment B, the goodness-of-fit (χ^2) parameter increased by 30%. The cluster size from this fit is estimated to $N = 923$ and the EAL becomes 14 Å, to be compared to the estimates of $N = 1415$ and EAL of 11 Å obtained in fits using the corrected PCI parameter. When comparing to the corresponding EAL estimate in C (19 Å) which is obtained using the correction, we note that the EAL estimate using the uncorrected parameter is still lower (14 Å). Thus the observation of longer EALs with larger cluster size holds under any reasonable assumption of size dependence of the correction factor proposed in Ref. [29].

APPENDIX B: ELECTRON BACKSCATTERING IN RARE GAS CLUSTERS

Figure 8 shows the FEFF calculations for argon clusters. In each of these clusters we chose to probe three different sites: the center atom, a vertex site at the surface, and a site just beneath the surface. In Fig. 9 the results of the FEFF calculation for

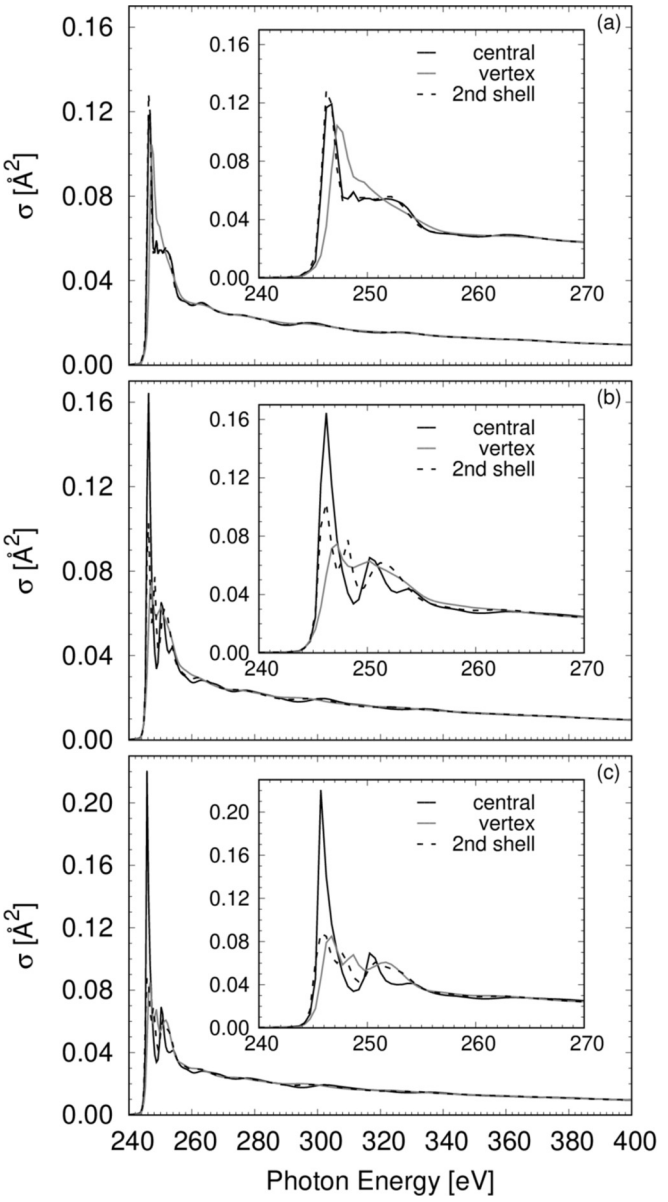

FIG. 8. Computed photoabsorption cross section σ as a function of photon energy for argon clusters. (a) $N = 55$, cuboctahedral-fcc; (b) $N = 55$, icosahedral; (c) $N = 147$, icosahedral. The insets show the regions close to threshold.

icosahedral clusters of krypton and xenon are shown. As it has been the case for argon clusters there are some differences in the photoionization cross section for surface and interior atoms in the cluster very close to the ionization threshold. This region extends to about 10 eV above threshold. At still higher photon energies the photoionization cross section of the different sites show only minor differences, especially in the case of xenon. For krypton relative differences in the cross section between the central atom and one at the vertex site can amount to about 10% in the region from 125 to 225 eV photon energy.

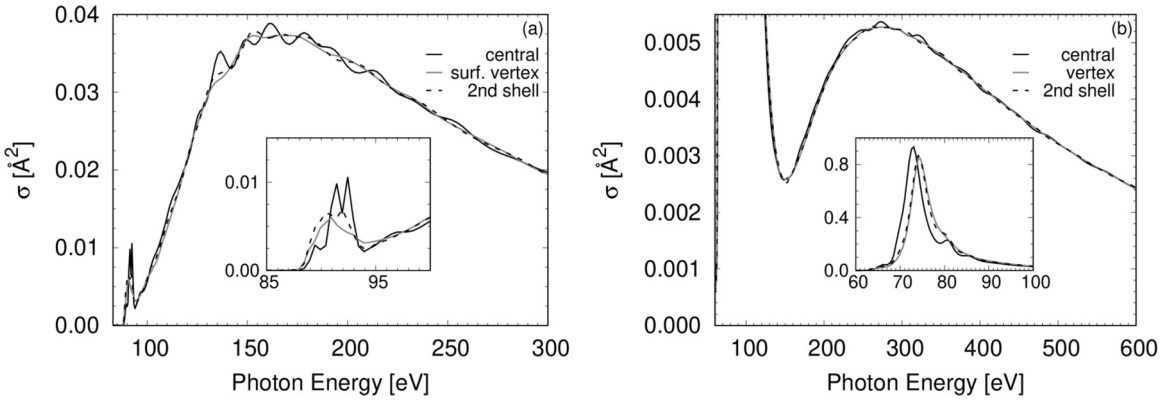

FIG. 9. Computed photoabsorption cross section σ as a function of photon energy for icosahedral clusters with 55 atoms of krypton (a) and xenon (b). The insets show the regions close to threshold.

[1] D. Briggs and J. T. Grant, *Surface Analysis by Auger and X-Ray Photoelectron Spectroscopy* (IMPublications, Chichester, UK, 2003).

[2] M. Gorgoi, S. Svensson, F. Schäfers, G. Öhrwall, M. Mertin, P. Bressler, O. Karis, H. Siegbahn, A. Sandell, H. Rensmo, W. Doherty, C. Jung, W. Braun, and W. Eberhardt, Nucl. Instrum. Methods A **601**, 48 (2009).

[3] C. J. Powell and A. Jablonski, *NIST Electron Inelastic-Mean-Free-Path Database* (National Institute of Standards and Technology, Gaithersburg, MD, 2000).

[4] C. J. Powell and A. Jablonski, *NIST Electron Effective-Attenuation-Length Database* (National Institute of Standards and Technology, Gaithersburg, MD, 2003).

[5] B. Boudaïffa, P. Cloutier, D. Hunting, M. A. Huels, and L. Sanche, Science **287**, 1658 (2000).

[6] J. D. Bourke and C. T. Chantler, Phys. Rev. Lett. **104**, 206601 (2010).

[7] K. Wittmaack, Phys. Rev. B **91**, 115434 (2015).

[8] N. Ottosson, M. Faubel, S. E. Bradforth, P. Jungwirth, and B. Winter, J. Electron Spectrosc. Relat. Phenom. **177**, 60 (2010).

[9] S. Thürmer, R. Seidel, M. Faubel, W. Eberhardt, J. C. Hemminger, S. E. Bradforth, and B. Winter, Phys. Rev. Lett. **111**, 173005 (2013).

[10] Y.-I. Suzuki, K. Nishizawa, N. Kurahashi, and T. Suzuki, Phys. Rev. E **90**, 010302 (2014).

[11] M. Michaud, A. Wen, and L. Sanche, Radiat. Res. **159**, 3 (2003).

[12] R. L. Kurtz, N. Usuki, R. Stockbauer, and T. E. Madey, J. Electron Spectrosc. Relat. Phenom. **40**, 35 (1986).

[13] M. Abu-samha and K. J. Børve, J. Phys. B: At. Mol. Opt. Phys. **46**, 025102 (2013).

[14] M. Winkler, V. Myrseth, J. Harnes, and K. J. Børve, J. Chem. Phys. **141**, 164305 (2014).

[15] R. Signorell, M. Goldmann, B. L. Yoder, A. Bodi, E. Chasovskikh, L. Lang, and D. Luckhaus, Chem. Phys. Lett. **658**, 1 (2016).

[16] M. Goldmann, J. Miguel-Sánchez, A. H. C. West, B. L. Yoder, and R. Signorell, J. Chem. Phys. **142**, 224304 (2015).

[17] M. Tchaplyguine, R. R. Marinho, M. Gisselbrecht, J. Schulz, N. Mårtensson, S. L. Sorensen, A. Naves de Brito, R. Feifel, G. Öhrwall, M. Lundwall, S. Svensson, and O. Björneholm, J. Chem. Phys. **120**, 345 (2004).

[18] F. G. Amar, J. Smaby, and T. J. Preston, J. Chem. Phys. **122**, 244717 (2005).

[19] J. Nordgren, H. Ågren, C. Nordling, and K. Siegbahn, Phys. Scr. **19**, 5 (1979).

[20] P. Ren and J. W. Ponder, J. Comput. Chem. **23**, 1497 (2002).

[21] P. Ren and J. W. Ponder, J. Phys. Chem. B **107**, 5933 (2003).

[22] J. Farges, M. de Feraudy, B. Raoult, and G. Torchet, Surf. Sci. **106**, 95 (1981).

[23] O. G. Peterson, D. N. Batchelder, and R. O. Simmons, Phys. Rev. **150**, 703 (1966).

[24] N. V. Krainyukova, R. E. Boltnev, E. P. Bernard, V. V. Khmelenko, D. M. Lee, and V. Kiryukhin, Phys. Rev. Lett. **109**, 245505 (2012).

[25] T. Ikeshoji, G. Torchet, M. F. deFeraudy, and K. Koga, Phys. Rev. E **63**, 031101 (2001).

[26] B. van de Waal, G. Torchet, and M.-F. de Feraudy, Chem. Phys. Lett. **331**, 57 (2000).

[27] M. Jurvansuu, A. Kivimäki, and S. Aksela, Phys. Rev. A **64**, 012502 (2001).

[28] P. van der Straten, R. Morgenstern, and A. Niehaus, Z. Phys. D **8**, 35 (1988).

[29] A. Lindblad, R. F. Fink, H. Bergersen, M. Lundwall, T. Rander, R. Feifel, G. Öhrwall, M. Tchaplyguine, U. Hergenhahn, S. Svensson, and O. Björneholm, J. Chem. Phys. **123**, 211101 (2005).

[30] K. B. Dyall, F. P. Larkins, K. Bomben, and T. D. Thomas, J. Phys. B **14**, 2551 (1981).

[31] E. Kukk, Spectral Analysis by Curve Fitting Macro Package SPANCF 2000, http://www.geocities.com/ekukk/intro.htm.

[32] J. J. Rehr, J. J. Kas, F. D. Vila, M. P. Prange, and K. Jorissen, Phys. Chem. Chem. Phys. **12**, 5503 (2010).

[33] O. F. Hagena, Z. Phys. D **4**, 291 (1987).

[34] U. Buck and R. Krohne, J. Chem. Phys. **105**, 5408 (1996).

[35] R. Karnbach, M. Joppien, J. Stapelfeldt, J. Wörmer, and T. Möller, Rev. Sci. Instrum. **64**, 2838 (1993).

[36] H. Lu, G. Ni, R. Li, and Z. Xu, J. Chem. Phys. **132**, 124303 (2010).

[37] K. C. Gupta, N. Jha, P. Deb, D. R. Mishra, and J. K. Fuloria, J. Appl. Phys. **118**, 114308 (2015).
[38] H. Bergersen, M. Abu-samha, A. Lindblad, R. R. T. Marinho, D. Céolin, G. Öhrwall, L. J. Sæthre, M. Tchaplyguine, K. J. Børve, S. Svensson, and O. Björneholm, Chem. Phys. Lett. **429**, 109 (2006).
[39] U. Hergenhahn, S. Barth, V. Ulrich, M. Mucke, S. Joshi, T. Lischke, A. Lindblad, T. Rander, G. Öhrwall, and O. Björneholm, Phys. Rev. B **79**, 155448 (2009).
[40] M. Förstel, M. Mucke, T. Arion, T. Lischke, S. Barth, V. Ulrich, G. Öhrwall, O. Björneholm, U. Hergenhahn, and A. M. Bradshaw, Phys. Rev. B **82**, 125450 (2010).
[41] M. Förstel, M. Mucke, T. Arion, T. Lischke, S. Barth, V. Ulrich, G. Öhrwall, O. Björneholm, U. Hergenhahn, and A. M. Bradshaw, J. Elec. Spectrosc. Relat. Phenom. **184**, 107 (2011).
[42] J. Farges, M. F. de Feraudy, B. Raoult, and G. Torchet, J. Chem. Phys. **78**, 5067 (1983).
[43] J. Farges, M. F. de Feraudy, B. Raoult, and G. Torchet, J. Chem. Phys. **84**, 3491 (1986).
[44] J. Cuvellier, P. Meynadier, P. de Pujo, O. Sublemontier, J.-P. Visticot, J. Berlande, A. Lallement, and J.-M. Mestdagh, Z. Phys. D: At., Mol. Clu. **21**, 265 (1991).
[45] R. S. Brusa, G. P. Karwasz, and A. Zecca, Z. Phys. D **38**, 279 (1996).
[46] R. Panajotović, D. Filipović, B. Marinković, V. Pejćev, M. Kurepa, and L. Vušković, J. Phys. B: At. Mol. Opt. Phys. **30**, 5877 (1997).
[47] C. J. Powell and A. Jablonski, J. Surf. Anal. **17**, 170 (2011).
[48] N. Schwentner, Phys. Rev. B **14**, 5490 (1976).
[49] E. Gargioni and B. Grosswendt, Rev. Mod. Phys. **80**, 451 (2008).
[50] G. G. Raju, IEEE Trans. Dielectr. Electr. Insul. **11**, 649 (2004).
[51] E. Keszei, V. Cobut, and J.-P. Jay-Gerin, J. Elec. Spectrosc. Relat. Phenom. **58**, 33 (1992).
[52] M. Lundwall, A. Lindblad, G. Öhrwall, S. Svensson, and O. Björneholm, Phys. Rev. A **78**, 065201 (2008).
[53] Y. Hikosaka, R. Mashiko, T. Odagiri, J. Adachi, H. Tanaka, T. Kosuge, and K. Ito, Phys. Rev. A **93**, 063412 (2016).
[54] W. Eberhardt, S. Bernstorff, H. W. Jochims, S. B. Whitfield, and B. Crasemann, Phys. Rev. A **38**, 3808 (1988).
[55] X. Feng, A. A. Wills, E. Sokell, T. W. Gorczyca, M. Wiedenhoeft, and N. Berrah, Phys. Rev. A **72**, 042712 (2005).
[56] T. Pflüger, A. Senftleben, X. Ren, A. Dorn, and J. Ullrich, Phys. Rev. Lett. **107**, 223201 (2011).
[57] F. Blanco and G. García, J. Phys.: Conf. Ser. **438**, 012012 (2013).
[58] N. Mårtensson, J. Söderstrom, S. Svensson, O. Travnikova, M. Patanen, C. Miron, L. J. Sæthre, K. J. Børve, T. D. Thomas, J. J. Kas, F. D. Vila, and J. J. Rehr, J. Phys.: Conf. Ser. **430**, 012131 (2013).
[59] L. Avaldi, G. Dawber, R. Camilloni, G. C. King, M. Roper, M. R. F. Siggel, G. Stefani, and M. Zitnik, J. Phys. B: At. Mol. Opt. Phys. **27**, 3953 (1994).
[60] N. Pauly and S. Tougaard, Surf. Sci. **604**, 1193 (2010).
[61] F. Yubero and S. Tougaard, Phys. Rev. B **71**, 045414 (2005).
[62] N. Pauly and S. Tougaard, Surf. Sci. **605**, 1556 (2011).
[63] G. Baldini, Phys. Rev. **128**, 1562 (1962).
[64] R. Ramirez and L. M. Falicov, Phys. Rev. B **1**, 3464 (1970).
[65] A. C. Newell and R. C. Baird, J. Appl. Phys. **36**, 3751 (1965).